Periodic Corrugations to Increase Efficiency of Thermophotovoltaic Emitting Structures

Youngjoon Hong,[1] Matthew Otten,[2] Misun Min,[3] Stephen K. Gray,[2] and David P. Nicholls[4]
[1)] *Department of Mathematics and Statisitcs, San Diego State University, San Diego, CA 92182, USA*
[2)] *Center for Nanoscale Materials, Argonne National Laboratory, 9700 South Cass Avenue, Lemont, IL 60439, USA*
[3)] *Mathematics and Computer Science Division, Argonne National Laboratory, 9700 South Cass Avenue, Lemont, IL 60439, USA*
[4)] *Department of Mathematics, Statistics, and Computer Science, University of Illinois at Chicago, 851 South Morgan Street, Chicago, IL 60607, USA*

In this letter we consider the question of designing insulator/metal thermovoltaic structures with periodically corrugated interfaces that give optimal performance based on the metric of useful power density. Using a Monte Carlo approach in a robust, rapid, and high-accuracy numerical simulation strategy, we have identified such interface shapes. We searched among the class of sinusoids and found that a flat-interface configuration could be significantly improved in transverse magnetic polarization. More specifically, we found that (i.) the performance improves with increasing corrugation amplitude (ii.) up to a maximum, (iii.) the shape of the corrugation is largely irrelevant, and (iv.) the period of the corrugation should be chosen in connection to the bandgap energy of the photovoltaic cell. For the latter we provide a simple expression as a starting point for practitioners interested in fabricating such structures.

Introduction. A thermophotovoltaic (TPV) emitter is a structure that, when heated to an appropriate temperature, emits photons with energies suitable for the generation of electricity by a photovoltaic (PV) cell.[1] If solar energy is used to heat the emitter, then the full system is a solar thermophotovoltaic (STPV) system,[1,2] although applications of TPVs involving nonsolar-based energy (e.g., waste heat) are also of great interest. Ideally, the emitted photons should have energies near and above the bandgap energy of the relevant PV cell. If the emitter were simply a blackbody emitter, then only the operating temperature would be of relevance; but layered and nanostructured TPV structures can lead to emission properties more tailored for efficient energy generation.[3,4]

Inspired by Jeon *et al*[5], we consider a simple Bragg reflector-tungsten TPV system (see Figure 1) and use

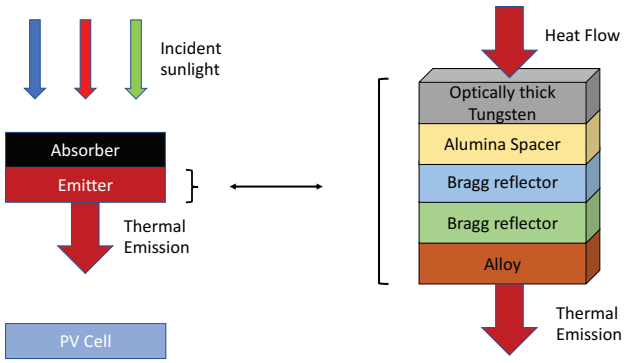

FIG. 1: Depiction of the full STPV system (left) with special emphasis on the TPV emitter structure (right).

a highly efficient computational electrodynamics procedure to predict optimal surface structuring. By corrugating the interfaces in the emitter we can enhance the emissivity in the relevant, sub-bandgap range of energies. We follow Ref. 6 where the authors reasoned that such corrugations act like a "graded" material and allow one to modify the emissivity. However, rather than consider their sharply varying sawtooth profiles[6], we focus on smooth periodic profiles to corrugate. Not only is this feature advantageous for our numerical algorithm, but also the response is similar to sawtooth shapes readily generated by modern fabrication techniques.

The numerical approach we utilize is a high-order perturbation of surfaces (HOPS) algorithm[7–10], which utilizes *surface* unknowns, giving it an orders-of-magnitude advantage in terms of storage and execution time over volumetric approaches such as finite difference,[11] finite element,[12] spectral element,[13] and spectral[14] methods. Furthermore, because of its perturbative character and expression in terms of periodic eigenfunctions of the Laplacian, it has advantages over integral equations approaches[15]: there is no need for specialized quadratures, periodization strategies, or iteration schemes for solving dense, nonsymmetric positive-definite systems of linear equations.[16,17]

From our simulations we have made a number of important discoveries. First, the introduction of periodic corrugations can *significantly* increase the useful power density (4.2651 W/cm^2 versus 3.4443 W/cm^2) of solar cells in transverse magnetic (TM) polarization. Second, the enhancement grows with increasing corrugation amplitude up to a maximal value beyond which the beneficial effects dissipate. Third, the *shape* of the corrugation does not appear to be crucial since a simple sinusoid produces roughly the same results as those produced by a sawtooth profile. Finally, our results improve as the period, d, of the corrugation is adapted to the bandgap

wavelength, λ_{BG}, of the underlying PV cell. Based upon careful study of the emissivity of our structures we have derived the rule $d \approx 2\pi/\lambda_{BG}$ as a useful starting point for practitioners building such devices. We note that our results depend strongly on polarization: The difference between flat and corrugated is minimal in transverse electric (TE) polarization, however, it is sizable in TM.

Governing Equations. Figure 2 displays the geometry of the configuration we consider: a y-invariant $(M+1)$-layered insulator-metal structure. An insulator (vacuum with refractive index $n_{vac} = 1$) occupies the domain *above* the uppermost interface $\{z > g_1(x)\}$ and metal (tungsten) fills $\{z < g_M(x)\}$. A tungsten-alumina alloy spacer (Al_2O_3 with $n_{al} = 1.7682$ with tungsten volume fraction $0 \le f_W \le 1$) occupies the second layer, $\{g_2(x) < z < g_1(x)\}$, while a Bragg reflector composed of alternating layers of SiO_2 ($n_{si} = 1.4585$) and TiO_2 ($n_{ti} = 2.6142$) occupies the middle of the structure $\{g_M(x) < z < g_2(x)\}$. We focus upon d-periodic grating interfaces, typically $g_j(x) = \bar{g}_j + a\sin(2\pi x/d)$, and work with triply layered Bragg structures so that $M = 5$. The

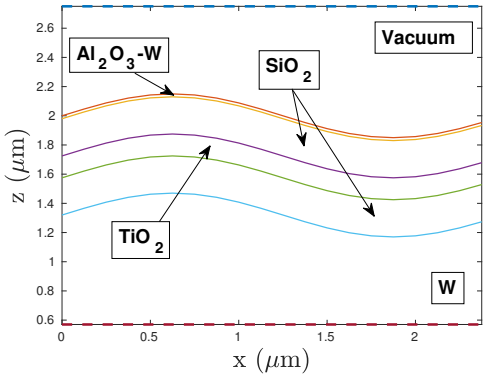

FIG. 2: Bragg-tungsten structure with sinusoidal periodic interfaces.

structure is illuminated from above by monochromatic plane-wave incident radiation of frequency ω, aligned with the grooves. Factoring out the common term $\exp(-i\omega t)$, we choose the reduced electric and magnetic fields as unknowns, which, like the incident field, are quasiperiodic.

In this two-dimensional setting the time-harmonic Maxwell equations decouple into $(M+1)$-many scalar Helmholtz problems that govern the TE and TM polarizations[18]. We denote the invariant (y) directions of the scattered (electric or magnetic) fields by $v_m(x,z)$ in layer m, and the incident radiation in the upper layer by v^i. We seek outgoing, quasiperiodic solutions of

$$\Delta v_m + \left(k^{(m)}\right)^2 v_m = 0, \quad g_{m+1}(x) < z < g_m(x), \tag{1}$$

$$v_{m-1} - v_m = -\delta_{m,1} v^i, \quad z = g_m(x), \tag{2}$$

$$\partial_{N_m} v_{m-1} - \tau_m^2 \partial_{N_m} v_m = -\delta_{m,1}\partial_{N_m} v^i, \quad z = g_m(x), \tag{3}$$

where $\delta_{m,\ell}$ is the Kronecker delta, $k^{(m)} = n^{(m)}\omega/c$, $N_m = (-\partial_x g_m, 1)^T$, $\tau_m^2 = 1$ in TE, and

$$\tau_m^2 = \left(k^{(m)}/k^{(m+1)}\right)^2 = \left(n^{(m)}/n^{(m+1)}\right)^2, \quad \text{in TM.}$$

The Rayleigh expansions[18,19] state, for $z > |g_1|_{L^\infty}$,

$$v_0(x,z) = \sum_{p=-\infty}^{\infty} \hat{a}_p e^{i\alpha_p x} e^{i\gamma_p^{(0)} z},$$

where $\alpha_p := \alpha + 2\pi p/d$, $\gamma_p^{(0)} = \sqrt{(k^{(0)})^2 - \alpha_p^2}$, with $\mathrm{Im}(\gamma_p^{(0)}) \ge 0$, and the "propagating modes" are $\mathcal{U}^{(0)} = \left\{p \in \mathbf{Z} \mid \alpha_p^2 < (k^{(0)})^2\right\}$. The emissivity (equal to the absorbance) is defined as

$$\epsilon_s(\lambda) = 1 - \sum_{p\in\mathcal{U}^{(0)}} e_p^{(0)}, \quad e_p^{(0)} := \frac{\gamma_p^{(0)} \left|(\widehat{v_0})_p\right|^2}{\gamma^{(0)}}.$$

Numerical Scheme. We follow a HOPS methodology to solve (1)–(3), which successively corrects the flat-interface (Fresnel) approximation.[8,16,20–22] The approach begins with the assumption that the shapes of the interface deformations g_m satisfy $g_m = \varepsilon f_m$ $(\varepsilon \ll 1)$ with f_m sufficiently smooth. The smallness assumption on ε can be removed by analytic continuation[23,24] and numerically implemented via Padé summation.[8,25,26]

We utilize the Transformed Field Expansions approach[8,20] which we recall here. A simple change of variables is effected in each layer which flattens the domain interfaces, $\{z = g_j(x)\}$ to $\{z' = \bar{g}_j\}$. This delivers equations for the transformed fields, $u_m(x',z') = v_m(x(x',z'), z(x',z'))$, e.g.,

$$\Delta' u_m + \left(k^{(m)}\right)^2 u_m = F_m(x',z'),$$

for (1), where forms for F_m can be readily derived.[9,10] Classical results[7,20] imply that the transformed fields depend *analytically* on the deformation size ε so that, e.g.,

$$u_m = u_m(x',z';\varepsilon) = \sum_{n=0}^{\infty} u_{m,n}(x',z')\varepsilon^n. \tag{4}$$

This expansion is inserted into the transformed version of (1)–(3) resulting in a system of coupled inhomogeneous Helmholtz problems governing the $u_{m,n}$ to be solved. For the purpose of approximating these, we have selected a

stable, High-Order Spectral Fourier-Legendre Galerkin approach[14] where

$$u_{m,n} \approx \sum_{p=-N_x/2}^{N_x/2-1} \sum_{\ell=0}^{N_z} \tilde{u}_{m,n,p,\ell} L_\ell(z) e^{i\alpha_p x},$$

and the L_ℓ are appropriately scaled and translated Legendre polynomials. For smooth profiles f_m, the scattered fields, u_m, are jointly analytic in x, z, and ε, so the coefficients $\tilde{u}_{m,n,p,\ell}$ decay exponentially fast as $\{m, n, p, \ell\}$ grow[8]. Thus, only a small number of these are required to deliver a high–fidelity solution which can be discovered very quickly. Naturally, as the deformation size ε becomes larger, more perturbation orders n are required which slows our algorithm.

Figure of Merit. A figure of merit that measures the utility of our structures comes from Planck's law for the spectral radiance of a black body at temperature T,

$$B(\lambda, T) = \left(\frac{4\pi\hbar c^2}{\lambda^5}\right) \frac{1}{\exp(Q) - 1}, \quad Q := \frac{2\pi\hbar c}{k_B T \lambda},$$

where $\hbar$ is Planck's constant, c is the speed of light in a vacuum, and k_B is the Boltzman constant. With this the (useful) *power density* is given by

$$P := \int_0^{\lambda_{BG}} \frac{\lambda}{\lambda_{BG}} B(\lambda, T) \epsilon_s(\lambda)\, d\lambda, \tag{5}$$

where we restricted the integration domain to be $\{\lambda_{min} < \lambda < \lambda_{max}\}$. Jeon *et al*[5] introduced a second figure of merit, the "spectral efficiency," which, in our simulations, decreased only slightly with the introduction of corrugations.

Numerical Results. In all of our simulations we chose the physical parameters $\lambda_{BG} = 2.254\ \mu m$, $\lambda_{min} = 0.6\ \mu m$, $\lambda_{max} = 6.0\ \mu m$, $T = 1700\ K$, and $f_W = 0.75$, where we have used a Maxwell formula to estimate the permittivity of the alloy.[5] Geometrically we have chosen the base layer thicknesses to be: 20 nm tungsten-alumina alloy, 255 nm SiO_2, and 150 nm TiO_2.

To begin we consider a selection of representative configurations with sinusoidal corrugations of spatial period, $d = 2.5\ \mu m$, and amplitudes $a = 0, 0.15, 0.275, 0.35\ \mu m$. The results are summarized in Table I. The final column, δ, is a dimensionless measure of the energy defect when the tungsten and alloy layers are replaced by a dielectric. If $\delta = 0$, then energy is perfectly conserved (as it should be in a dielectric structure), while values of 10^{-2} to 10^{-3} indicate that 2-3 digits can be trusted. From this table we learn a number of things. First, we can increase the useful power density by nearly 25 % with the introduction of periodic sinusoidal corrugations. To see why this is the case we display, in Figure 3 the emissivity, ϵ_s, for flat ($a = 0\ \mu m$) and corrugated ($a = 0.25\ \mu m$) interface configurations. We notice the significant enhancement to the magnitude of the emissivity below the bandgap wavelength in the presence of corrugations. In addition, from

TABLE I: Numerical results for six-layer structures.

$a(\mu m)$	PD (W/cm^2)	δ	N_x	N_z	N
0	3.4443	4×10^{-16}	20	20	20
0.15	3.8381	3×10^{-3}	20	20	20
0.275	4.2651	8×10^{-3}	20	40	40
0.35	4.1651	1×10^{-2}	20	40	40

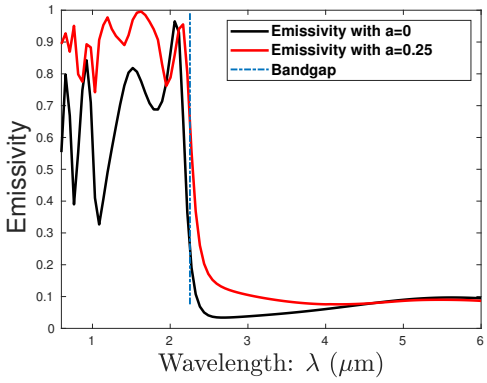

FIG. 3: Plot of the emissivity, ϵ_s, versus wavelength, λ, for the sinusoidally corrugated interface configuration with $a = 0, 0.25\ \mu m$. ($N_x = N_z = 20$ and $N = 20$.)

Table I we note that the improvement in useful power density increases as the corrugation amplitude increases to a maximum around $a \approx 0.275\ \mu m$, but then decreases again as a increases.

To discern the effect of the particular *shape* of the interface deformations, we ran these simulations again with $a = 0.18\ \mu m$ and interfaces shaped as sawtooth profiles (see Figure 4). These simulations revealed that the useful

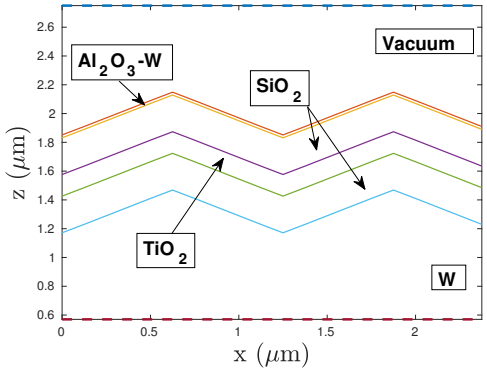

FIG. 4: Bragg-tungsten structure with sawtooth periodic interfaces.

power density increases from 4.01 W/cm^2 to 4.03 W/cm^2

when the sharp sawtooth corrugations are introduced, which is clearly not significant.

Continuing, we decided to investigate the possibility of improving the performance of our design by varying the *period* of our corrugations. For this we selected 100 samples of d from the uniform distribution $U(1.6, 3.0)$ (in microns) for a fixed amplitude $a = 0.18\ \mu m$; the results are depicted in Figure 5. Here we see a signif-

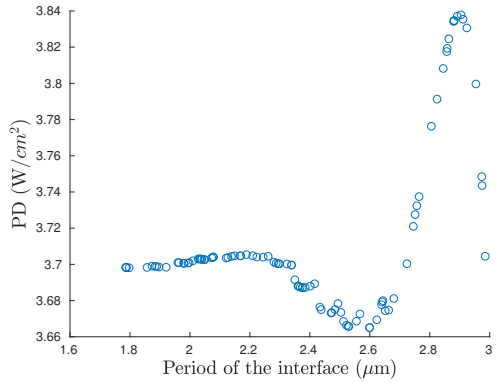

FIG. 5: Useful power density versus period of the sinusoidally corrugated interfaces. ($N_x = N_z = 20$ and $N = 20$.)

icant *spike* near the value $d = 2.8\ \mu m$. Our explanation for this result is that it is within a small neighborhood of $2\pi/\lambda_{BG} \approx 2.7876$ so that our emissivity profile is tailored to the bandgap of the PV. To make this more quantitative we display the emissivity for a period d near this critical value $2\pi/\lambda_{BG}$ in Figure 6 ($d = 2.88$) and below/above ($d = 2.4, 3.2$) this value in Figure 7 with amplitude $a = 0.18\ \mu m$ corrugations. Here we

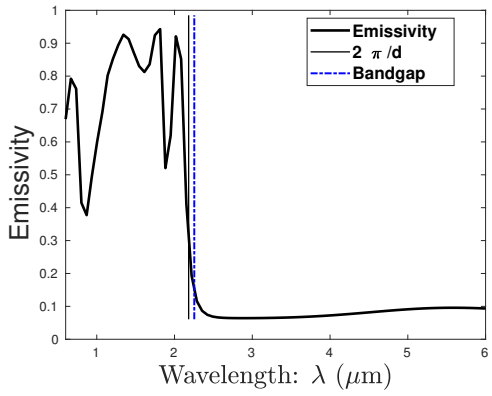

FIG. 6: Emissivity versus wavelength for period $d = 2.88\ \mu m$ ($d \approx 2\pi/\lambda_{BG}$) corrugated interfaces. ($N_x = N_z = 20$ and $N = 20$.)

see how the emissivity curve is "optimal" in the case $d = 2.88 \approx 2\pi/\lambda_{BG}$ case with all of the plasmonic peaks

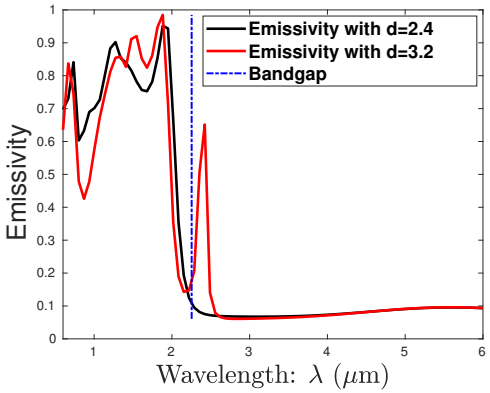

FIG. 7: Emissivity versus wavelength for periods $d = 2.4\ \mu m$ ($d < 2\pi/\lambda_{BG}$) and $d = 3.2\ \mu m$ ($d > 2\pi/\lambda_{BG}$) corrugated interfaces. ($N_x = N_z = 20$ and $N = 20$.)

located at wavelengths up to, but not past, the bandgap wavelength. By contrast, for $d < 2\pi/\lambda_{BG}$ the peaks do not exist all the way up to the bandgap wavelength, while for $d > 2\pi/\lambda_{BG}$ there are "wasted" peaks beyond.

Conclusions. In this letter we addressed the problem of designing TPV emitters consisting of Bragg reflectors overlaying tungsten with periodically corrugated interfaces. Using a rapid and robust HOPS solver, we have found such structures using the useful power density figure of merit. We determined that corrugations of simple sinusoidal form can give significant enhancements which grow with increasing amplitude up to a maximal value. The shape of the corrugation did not appear to be particularly important, however, the period, d, should be adapted to the bandgap wavelength of the PV cell, λ_{BG}, with a useful first approximation expressed by $d \approx 2\pi/\lambda_{BG}$.

We note that our calculations focus on normal incidence (emission), which is common in the literature. As discussed in the Supporting Information of Ref. 5, although angles near normal are expected to be most important, a more complete calculation would involve integrating over all angles of emission. The conditions for plasmonic/diffractive resonances depend on angle (e.g., eqns (1)–(2) of Ref. 27) so that there will likely be some deterioration in the overall power densities.

This paper has focused on achieving emissivities that can enhance power density associated with a PV cell at a particular band–gap energy. However, another important aspect of solar energy related problems (e.g., concentrating solar power[28]) is to design structures that can absorb over the entire solar spectrum. Figure 7 shows that one can achieve absorption (emissivity) at somewhat longer wavelengths by increasing the periodicity. The extent to which one could optimize the periodicity represents an interesting problem that we plan to address.

Acknowledgments. We thank J. Foley for helpful

discussions. This material is based upon work supported by the U.S. Department of Energy, Office of Science, Office of Advanced Scientific Computing Research, under Contract DE-AC02-06CH11357, and the National Science Foundation through grant No. DMS-1522548 (D.P.N.). Use of the Center for Nanoscale Materials, an Office of Science user facility, was supported by the U.S. Department of Energy, Office of Science, Office of Basic Energy Sciences, under Contract No. DE-AC02-06CH11357.

[1] P. Bermel, M. Ghebrebrhan, W. Chan, Y. X. Yeng, M. Araghchini, R. Hamam, C. H. Marton, K. F. Jensen, M. Soljacic, J. D. Joannopoulos, S. G. Johnson, and I. Celanovic, Opt. Express **18**, A314 (2010).
[2] S. Fan, Nat. Nanotechnol. **9**, 92 (2014).
[3] C. Ungaro, S. K. Gray, and M. C. Gupta, Appl. Phys. Lett. **103**, 071105 (2013).
[4] J. J. Foley, C. Ungaro, M. C. Gupta, and S. K. Gray, Opt. Express **23**, A1373 (2015).
[5] N. Jeon, J. Hernandez, D. Rosenmann, S. Gray, A. Martinson, and J. Foley, Advanced Energy Materials , 1801035 (2018).
[6] C. Ungaro, S. Gray, and M. Gupta, Optics Letters **39**, 5259 (2014).
[7] D. P. Nicholls and F. Reitich, Proc. Roy. Soc. Edinburgh Sect. A **131**, 1411 (2001).
[8] D. P. Nicholls and F. Reitich, J. Opt. Soc. Am. A **21**, 606 (2004).
[9] Y. Hong and D. P. Nicholls, Journal of Computational Physics **330**, 1043 (2017).
[10] Y. Hong and D. P. Nicholls, Journal of Computational Physics **345**, 162 (2017).
[11] R. J. LeVeque, *Finite difference methods for ordinary and partial differential equations* (Society for Industrial and Applied Mathematics (SIAM), Philadelphia, PA, 2007) pp. xvi+341, steady-state and time-dependent problems.
[12] C. Johnson, *Numerical solution of partial differential equations by the finite element method* (Cambridge University Press, Cambridge, 1987) p. 278.
[13] M. O. Deville, P. F. Fischer, and E. H. Mund, *High-order methods for incompressible fluid flow*, Cambridge Monographs on Applied and Computational Mathematics, Vol. 9 (Cambridge University Press, Cambridge, 2002) pp. xxviii+499.
[14] J. Shen, T. Tang, and L.-L. Wang, *Spectral methods*, Springer Series in Computational Mathematics, Vol. 41 (Springer, Heidelberg, 2011) pp. xvi+470, algorithms, analysis and applications.
[15] D. Colton and R. Kress, *Inverse acoustic and electromagnetic scattering theory*, 2nd ed. (Springer-Verlag, Berlin, 1998) pp. xii+334.
[16] D. P. Nicholls, Journal of the Optical Society of America, A **32**, 701 (2015).
[17] D. P. Nicholls, SIAM Journal on Numerical Analysis **55**, 144 (2017).
[18] R. Petit, ed., *Electromagnetic theory of gratings* (Springer-Verlag, Berlin, 1980) pp. xv+284.
[19] P. Yeh, *Optical waves in layered media*, Vol. 61 (Wiley-Interscience, 2005).
[20] D. P. Nicholls and F. Reitich, J. Opt. Soc. Am. A **21**, 590 (2004).
[21] D. P. Nicholls, F. Reitich, T. W. Johnson, and S.-H. Oh, Journal of the Optical Society of America, A **31**, 1820 (2014).
[22] D. P. Nicholls, S.-H. Oh, T. W. Johnson, and F. Reitich, Journal of Optical Society of America, A **33**, 276 (2016).
[23] D. P. Nicholls and F. Reitich, Numer. Math. **94**, 107 (2003).
[24] B. Hu and D. P. Nicholls, Proceedings of the Royal Society of Edinburgh A **140**, 367 (2010).
[25] O. Bruno and F. Reitich, J. Opt. Soc. Am. A **10**, 2307 (1993).
[26] D. P. Nicholls and F. Reitich, J. Comput. Phys. **170**, 276 (2001).
[27] H. Gao, J. M. McMahon, M. H. Lee, J. Henzie, S. K. Gray, G. C. Schatz, and T. W. Odom, Optics Express **17**, 2334 (2009).
[28] C. K. Ho, Solar Energy **152**, 38 (2017).